Hindawi
International Journal of Antennas and Propagation
Volume 2022, Article ID 9645280, 11 pages
https://doi.org/10.1155/2022/9645280

Research Article

An Omni-Directional Wideband Patch Antenna with Parasitic Elements for Sub-6 GHz Band Applications

Liton Chandra Paul,[1] **Himel Kumar Saha**,[1] **Tithi Rani**,[2] **Md. Zulfiker Mahmud**,[3] **Tushar Kanti Roy**,[2] **and Wang-Sang Lee**[4]

[1]*Department of EECE, Pabna University of Science and Technology, Pabna, Bangladesh*
[2]*Department of ETE, Rajshahi University of Engineering and Technology, Rajshahi, Bangladesh*
[3]*Department of CSE, Jagannath University, Dhaka, Bangladesh*
[4]*Department of Electronic Engineering, Gyeongsang National University, Jinju, Republic of Korea*

Correspondence should be addressed to Liton Chandra Paul; litonpaulete@gmail.com

Received 5 August 2022; Revised 16 September 2022; Accepted 19 September 2022; Published 4 October 2022

Academic Editor: Shah Nawaz Burokur

An omni-directional inset fed wideband microstrip patch antenna (MPA) for Sub-6 GHz applications has been presented. Initially, a slotted small patch antenna with a full ground plane is designed and then partial ground plane and electromagnetically coupled parasitic elements have been incorporated and optimized to get desired performance. The volume of the studied antenna is $40 \times 40 \times 1.575\ mm^3$ having a partial ground plane. Rogers RT 5880 is used as the dielectric substrate tier. The simulated operating band of the MPA ranges from 2.67 GHz to 4.20 GHz, covering the N77 and N78 bands with a centre operating frequency of 3.29 GHz. The antenna can also be used for WiMAX rel 2 (3.4–3.6 GHz) applications. After fabrication and testing, the antenna also shows almost the same working band extending from 2.67 GHz to 4.15 GHz. The use of a partial ground plane plays a vital role in making it an omni-directional antenna, and the existence of a rectangular parasitic element in the ground plane influences the improvement of gain and directivity of the antenna. The designed MPA allows it to run as a wide band antenna with a good reflection coefficient profile, high average efficiency, and $1 < VSWR < 2$. At a resonant tip of 3.29 GHz, the simulated gain and directivity are 3.16 dB and 3.38 dBi, respectively. The measured gain is slightly higher than the simulated gain. The computer simulation technology (CST) is used for modelling and exploring all the performance matrices of the antenna. The results of the fabricated prototype present very good similarity with the simulated results and both simulated and measured results also support the Sub-6 GHz band. The antenna prototype shows a very well balanced set of radiation characteristics with a miniaturized volume and high efficiency. Therefore, the inset fed MPA can be contemplated as a candid model for Sub-6 GHz band applications.

1. Introduction

Industrial revolution in wireless technology has become incontestable by the exponentially increasing number of wireless communication users. To meet the demand of huge data rates in wireless handy applications, technology has jumped from 2G to 3G, 3G to 4G, and 4G to 5G very rapidly and further developing day by day. The wireless communication researchers are also trying to conceptualize 6G technology. The 4th generation technology has evolved into 5G technology to issue a higher data rate, larger bandwidth, and minor delay since 2019 [1]. In packet switched wireless systems, a large bandwidth is used in 5G cell phones today. The 5 G provides data rate bigger than 100 Mbps at ultimate mobility and greater than 1 Gbps at meagre mobility [2]. The data rate varies from 5 Gbps up to 50 Gbps which is promised by 5G technology. To fulfil the criteria towards 2020, ITU provided 5G frequency bands that include N77 (3.3–4.2 GHz), N78 (3.3–3.8 GHz), and N79 (4.4–5.0 GHz) bands [3]. The low cost, low power level, lower consumed battery, and higher data rate motivate the

communication engineers to establish the efficient and widespread utilization of 5G technology. Microstrip slotted antennas are broadly used for wireless communications including WiMAX, WLAN, WPAN, LTE, Bluetooth, ISM, WiFi, 3G, 4G, and 5G applications [4–7]. The ITU provides different 5G bands for different countries. In the USA, 3.1–3.55 GHz and 3.7–4.2 GHz are used as the Sub-6 5G band. For Europe, 3.4–3.8 GHz is considered. In China, 3.3–3.6 GHz and 4.8–4.99 GHz bands have been allocated for 5G applications [8]. Microstrip patch antenna (MPA) is more preferable in the spectrum of wireless communication because of their low cost, light weight, stable radiation pattern, and high gain. The inset feeding technique, coplanar waveguide, partial ground plane, defected ground structure, slotted patch, and different shaped patch are applied to improve the performance of an antenna [9, 10]. An ultrawideband antenna is illustrated in Ref. [11]. Though the bandwidth of the antenna is excellent and it ranges from 3.05 GHz to 5.82 GHz, the efficiency and gain are very unstable over the bandwidth. The gain remains negative approximately up to 4.5 GHz and efficiency is also lower than 60% up to 5.5 GHz. In Ref. [12], a slotted antenna is proposed. The wide bandwidth is produced by the antenna having a maximum gain of 2.69 dB. The antenna is capable of serving 5G, WiMAX, WLAN, and 4G applications. A compact monopole patch antenna is described in Ref. [13]. The size of the antenna is $30 \times 34\ \text{mm}^2$. The antenna has a very good coverage for the Sub-6 band with a reflection coefficient of −50 dB. A rose-like patch antenna ($20 \times 35 \times 0.79\ \text{mm}^3$) with a slotted partial ground plane for Sub-6 GHz is proposed in Ref. [14]. For designing ultrawide band MPA, CST software is used in Ref. [15]. The bandwidth of the proposed RMPA is 2.32 GHz–5.24 GHz. The antenna is suitable for the Chinese 5G operating band. The gains are 2.52 dB at 2.55 GHz, 3.04 dB at 3.5 GHz, and 4.31 dB at 4.75 GHz. The antenna is also applicable for WiFi, Bluetooth, and WLAN communication which is an advantage of the antenna. In Ref. [16], a flexible antenna is proposed. Rogers 5880 is used as a flexible substrate. For 5 G, the MPA resonates at 3.5 GHz with a gain and efficiency of 2.51 dB and 92.7%, respectively. For the ISM band, the antenna resonates at 2.45 GHz with a gain of 1.74 dB and efficiency of 94%. In Ref. [17], a hexagonal-shaped antenna is described. A CPW feeding technique is used in the proposed antenna. The antenna is applicable for both WLAN and Sub-6 GHz applications. The gain of the antenna is poor (>1.5 dB), and the efficiency is greater than 85%. A concept of metamaterial is applied to enhance the performance of antennas [18, 19]. In Ref. [20], a compact MPA is described. The antenna is square shaped, having a bandwidth ranging from 3.4 to 3.6 GHz. The antenna is preferable for only the N78 band and not applicable for the N77 and N79 band. A Rogers RT 5880 based slotted monopole planar array for Sub-6 GHz is described in Ref. [21]. In Ref. [22], a large antenna having size of $40 \times 60 \times 1.52\ \text{mm}^3$ and efficiency of 80% has been discussed for 5G application. A dual band antenna with low bandwidth is described in Ref. [23]. Similarly, many antennas for Sub-6 GHz 5G applications with comparatively higher volume and lower efficiency have been studied in Refs. [24–34].

A compact ($40 \times 40 \times 1.575\ \text{mm}^3$) antenna with comparatively stable gain (Simulated: 1.95 dB to 3.92 dB and Measured: 2.45 dB to 3.51 dB) and directivity (2.97 dBi to 4.08 dBi) as well as having a high average radiation efficiency over the whole operating frequency range of Sub-6 GHz band application is analyzed briefly. The paper has been organized as follows: Section 2 elucidates the structure of omni-directional inset fed wideband microstrip patch antenna (MPA). All the simulated and measured outcomes are critically analyzed in section 3, and at last, conclusion of the presented work has been drawn at section 4.

2. Structure of the Inset Fed MPA

The geometrical formation of the proposed omni-directional inset-fed MPA with a partial ground plane for Sub-6 GHz band application is described in detail in this section. The antenna has three tiers, namely, ground, patch, and substrate. A fragment of Rogers RT 5880 material (2.2, 0.0009) is exercised for the antenna. The copper (annealed) is used for both patch and ground plane of the MPA. The thickness of Rogers RT 5880 and copper are 1.575 mm and 0.035 mm, respectively. Initially the size of the antenna has been estimated by using some fundamental equations (1)–(4) and then the greatness of the MPA is optimized to 40 mm × 40 mm × 1.575 mm by using CST-MWS.

$$\text{Patch width, } W_P = \frac{c}{2f_r}\sqrt{\frac{2}{\varepsilon_r + 1}}, \tag{1}$$

where c = velocity of light, f_r = resonance frequency, and ε_r = dielectric constant.

$$\text{Length, } L = 0.412h\frac{\left(\varepsilon_{reff} + 0.3\right)\left(W_p/h + 0.264\right)}{\left(\varepsilon_{reff} - 0.258\right)\left(W_p/h + 0.8\right)}, \tag{2}$$

$$\text{Effective length, } L_{eff} = \frac{c}{2f_r\sqrt{\varepsilon_{reff}}}, \tag{3}$$

$$\text{Patch length, } L_p = L_{eff} - 2\Delta L. \tag{4}$$

Figures 1(a) and 1(b) exhibits the top and back view with necessary labelling. The 3D view and fabricated prototype are presented in Figures 1(c) and 1(d), respectively. The width and length of the patch are $W_p = 10$ mm and $L_p = 9$ mm. There is a rectangular slot on the patch having width (W_s) and length (L_s) of 8 mm and 6 mm, respectively. The size of the inset is 1 mm × 2 mm. There are two rectangular shaped parasitic elements besides each side of the patch having a width (x) of 11 mm and length (m) of 22 mm. These parasitic elements influence the reflection coefficient as well as the efficiency of the antenna. The intervening space between two parasitic elements (d) is 12 mm. The width (W_f) and length (L_f) of the feeder are 4.8 mm and 18 mm, respectively. The MPA has a partial

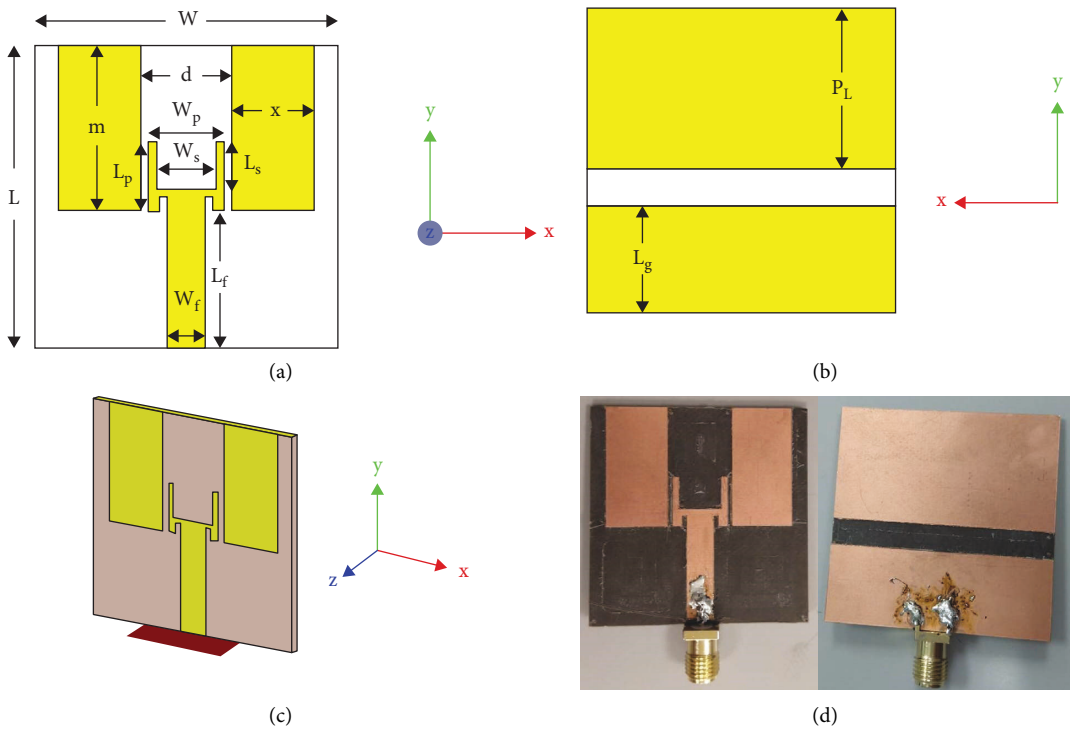

Figure 1: Proposed microstrip patch antenna (MPA). (a) Top view. (b) Back view. (c) 3D view. (d) Fabricated prototype.

ground plane, and the length of the partial ground plane (L_g) is 14 mm and a parasitic element has a length (P_L) of 21 mm. Actually, the lower part of the back side of the antenna acts as a partial ground plane and the upper part which is electrically separated but electromagnetically connected acts as a parasitic element. The partial ground plane aids to set the antenna omni-directional and rectangular parasitic elements enhance the directivity of the MPA over the exhaustive working Sub-6 GHz frequency band. The effective impedance of the antenna is completely matched with 50 Ω port impedance. The enumerated extent of excitation coefficient (k) is 4.6 to 8.68, and ultimately the worth of k has been optimized to 4.6 for the proposed MPA. All the designed factors are charted in Table 1.

Table 1: List of the factors of designed MPA.

Name and symbol	Weight (mm)
Length (L)	40
Width (W)	40
Thickness of Rogers RT 5880 (h)	1.575
Thickness of copper (t)	0.035
Patch's length (L_p)	9
Patch's width (W_p)	10
Length of slot (L_s)	6
Width of slot (W_s)	8
Length of the parasitic element on the patch (m)	22
Width of the parasitic element on the patch (x)	11
Distance between two parasitic elements of patch (d)	12
Feeder's length (L_f)	18
Feeder's width (W_f)	4.8
Length of parasitic element on ground plane (P_L)	21
Ground plane's length (L_g)	14

3. Results and Discussion

At first the fabricated MPA is designed and optimized by using CST-MWS and then fabricated and tested in the antenna laboratory. The simulated and measured scattering parameter (S_{11}-parameter) of an omni-directional microstrip patch antenna (MPA) is displayed in Figure 2. The S_{11} parameter is measured by using a vector network analyzer (VNA). The antenna is resonated at a frequency of 3.29 GHz with a simulated reflection coefficient of −33.69 dB and measured reflection coefficient of −25 dB. The simulated and measured operating frequency coverage ranges of the proposed antenna are 2.67 GHz to 4.20 GHz and 2.67 GHz to 4.15 GHz. Therefore, the measured and simulated bandwidths are 1.48 GHz and 1.53 GHz at the −10 dB point of the scattering parameter curve. The bandwidth is quite good for Sub-6 GHz bands (covering N77 and N78 bands). The antenna can also be useful for WiMAX rel 2 (3.4 GHz–3.6 GHz). Different countries use different Sub-6 GHz 5G bands. The designed antenna covers 5G bands of many countries such as 3.1–3.55 GHz and 3.7–4.2 GHz bands of USA, 3.4–3.8 GHz band of Europe, 3.6–3.8 GHz band of Spain, 3.3–3.6 GHz band of China, 3.4–3.8 GHz band of Ireland, 3.6–4.2 GHz band of Japan, 3.4–3.7 GHz band of Korea, 3.3–3.4 GHz band of India. The variation of the reflection coefficient for different lengths of parasitic element on the ground plane (P_L) as well as without parasitic element is shown in Figure 3. The return loss is higher without a parasitic element on the ground plane, and its

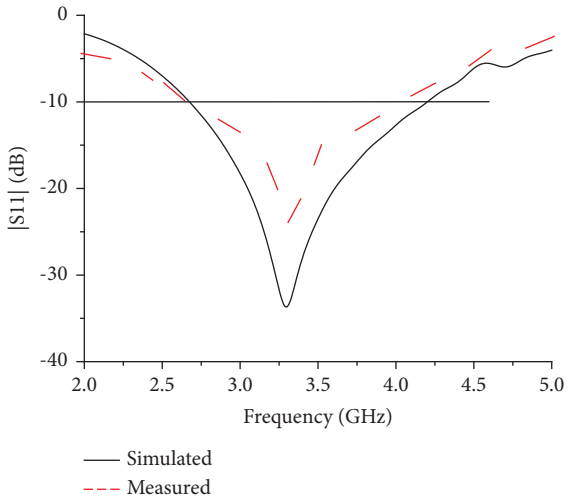

Figure 2: S_{11} curve of the designed MPA.

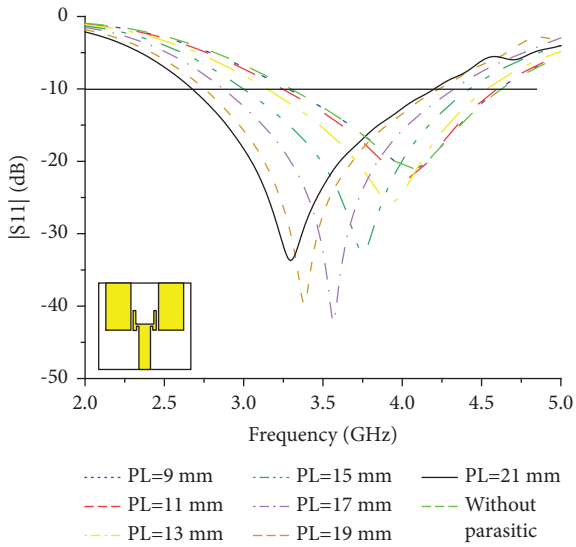

Figure 3: Variation of the reflection coefficient for different length of parasitic element on the ground plane (P_L).

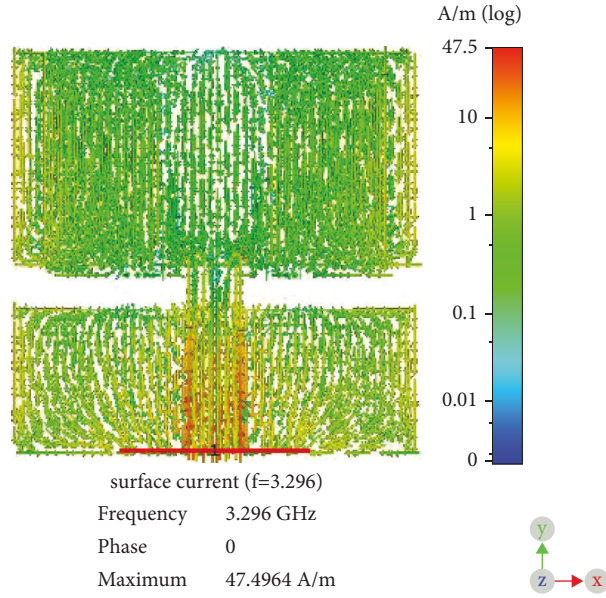

Figure 4: Surface current of the MPA at 3.296 GHz.

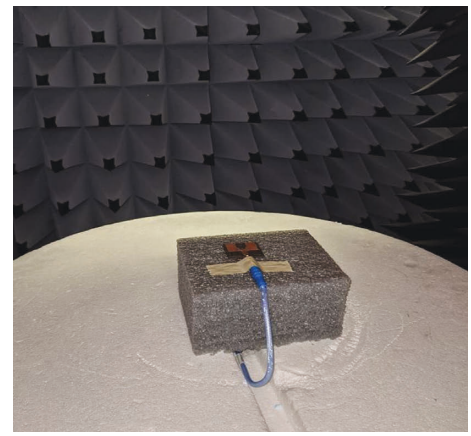

Figure 5: Fabricated prototype within the anechoic chamber.

centre frequency is 4.1 GHz. When the length (P_L) is varied from 9 mm to 21 mm with step size of 2 mm, the bandwidth of the antenna is slowly switched to the left side and the return loss is enhanced. The current flow on the surface of the microstrip patch antenna (MPA) at 3.29 GHz is illustrated in Figure 4 and the current is 47.49 A/m. The current distribution is slightly high at both left and right edges of the rectangular parasitic elements, and it is maximum at lower part of the antenna especially near the feeder of the MPA. Figure 5 represents the fabricated antenna setup within the anechoic chamber for radiation characteristics measurement. The polar and 3D representation of both gain and directivity are at 3.296 GHz, and linear gain and directivity graph over the exhaustive operating bandwidth of the inset fed MPA are illustrated in Figures 6(a)–6(f). At 3.29 GHz, the gain and directivity are 3.16 dB and 3.38 dBi. From Figure 6(e), the gain and directivity vary from 1.95 dB to 3.92 dB and 2.97 dBi to 4.08 dBi. The measured and simulated gain of the inset fed MPA are also compared in Figure 6(f). The measured gain also varies from 2.45 dB to 3.51 dB. There is a good compliance between the measured gain and simulated gain of the designed inset fed MPA prototype.

The gain of MPA increases by increasing the length (m) and width (x) of the parasitic element on the patch as depicted in Figure 7 and Figure 8, respectively. The gain of the antenna also increases with increasing the length of the parasitic element on the ground plane (P_L), as displayed in Figure 9. The MPA shows maximum gain for $m = 22$ mm, $x = 11$ mm, and $P_L = 21$ mm.

The polar scheme illustrations of the radiation pattern of the fabricated MPA for $\phi = 0^\circ$ and 90° at 3.29 GHz are depicted in Figure 10. From the pattern, the principal lobe is guided at 180° at $\phi = 0^\circ$ and 178° at $\phi = 90^\circ$. For both the

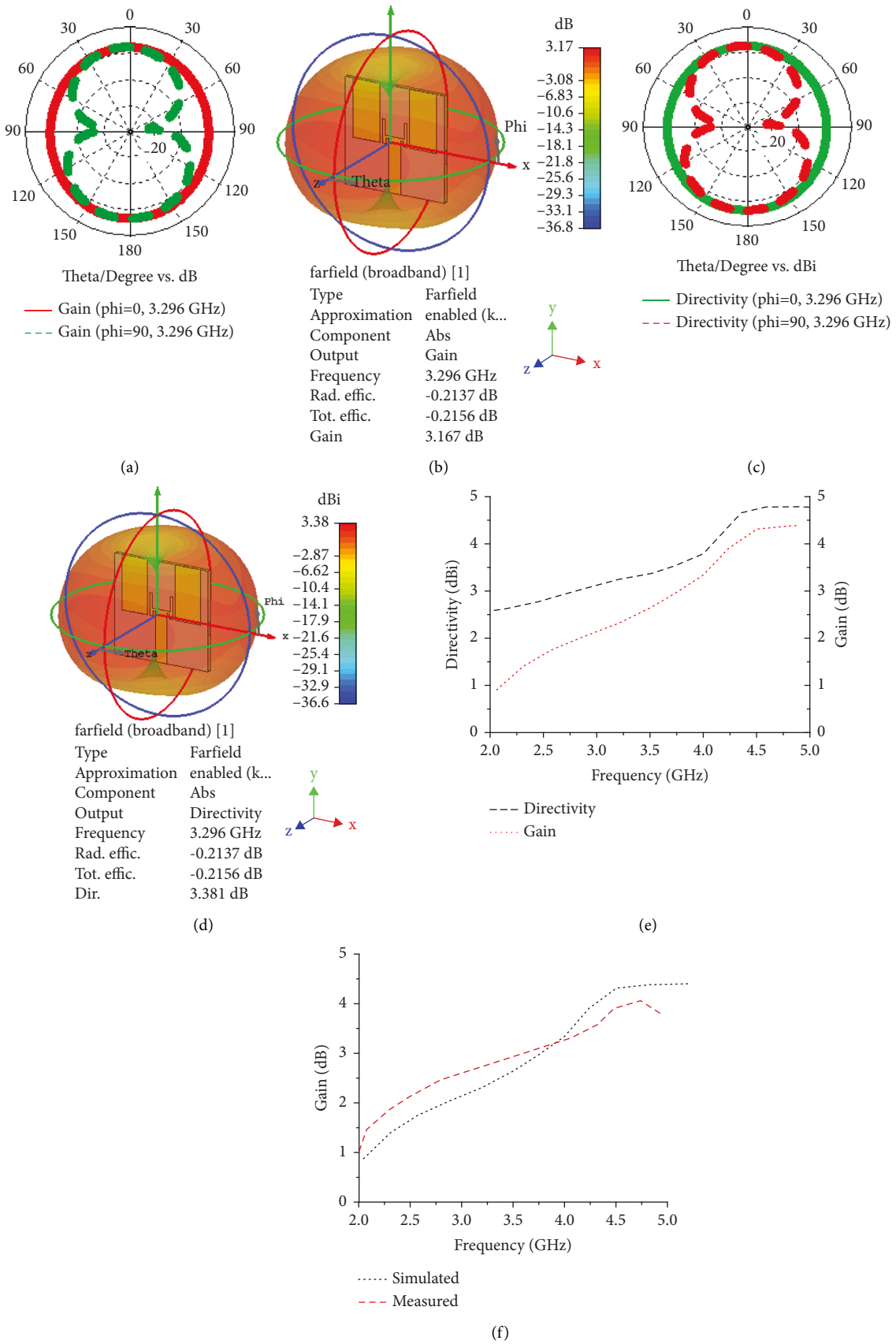

Figure 6: Gain and directivity of the inset fed MPA. (a) Gain (polar). (b) Gain (3D). (c) Directivity (polar). (d) Directivity (3D). (e) Simulated gain and directivity. (f) Simulated and measured gain.

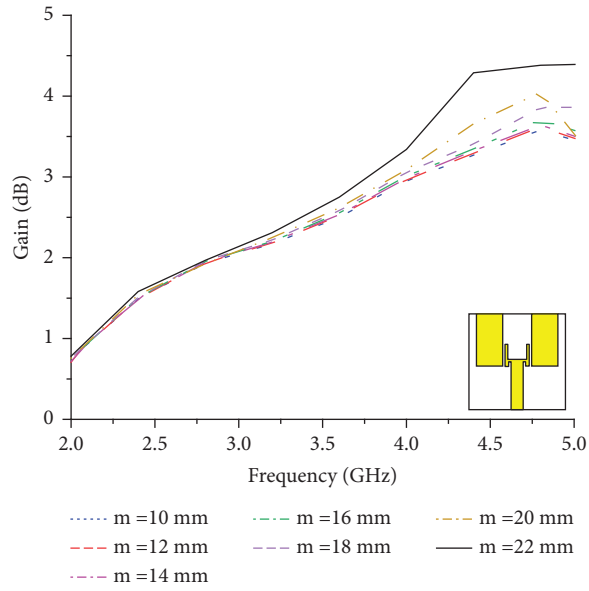

Figure 7: Variation of the gain for different length of parasitic element on patch (m).

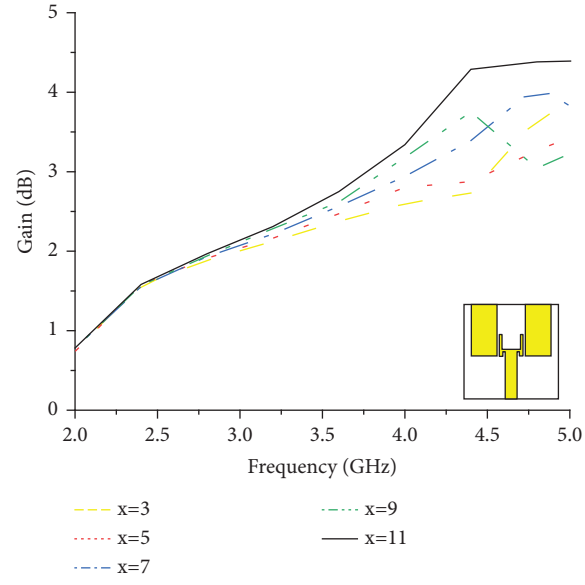

Figure 8: Variation of the gain for different width of the parasitic element on the patch (x).

electric and magnetic field, half power beam width (HPBW) or 3 dB angular beam width is 171° at $\phi = 0°$ and 83.4 at $\phi = 90°$. The main lobe magnitudes are 17.9 dBV/m at both $\phi = 0°$ and $\phi = 90°$ (for E-field); similarly, the main lobe magnitudes are −33.6 dBA/m at both $\phi = 0°$ and $\phi = 90°$ (for the H-field). The voltage standing wave ratio (VSWR) of the MPA prototype is displayed in Figure 11. From the figure, both the measured VSWR and simulated VSWR of the fabricated prototype are $1 < \text{VSWR} < 2$. The simulated and measured values are 1.04 and 1.32, respectively, at resonant points which are near to unity, revealing good port impedance matching property of the proposed MPA. The impact of the length of the parasitic element of the ground plane (P_L) on VSWR has been studied in Figure 12. The antenna shows the best VSWR for $P_L = 21$ mm.

For any antenna, efficiency is the ability of being able to emit EM signals successfully. A linear representation of measured and simulated efficiency graph is incorporated in Figure 13. The antenna shows good efficiency. There is a

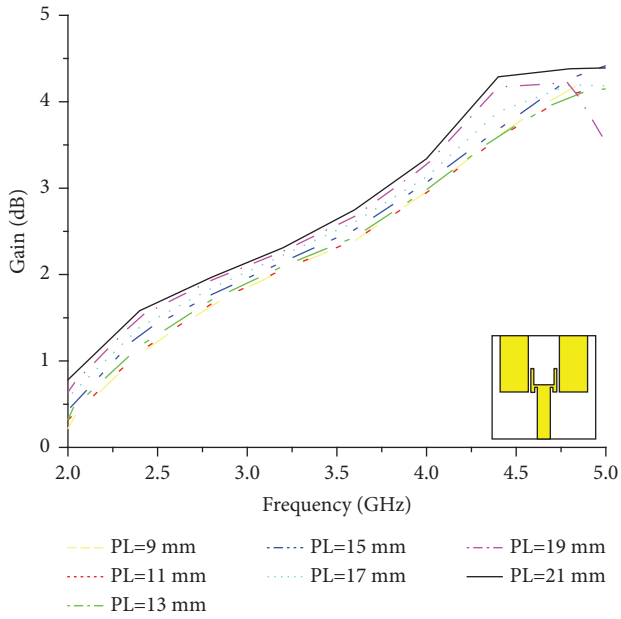

Figure 9: Variation of the gain for different length of parasitic element on the ground plane (P_L).

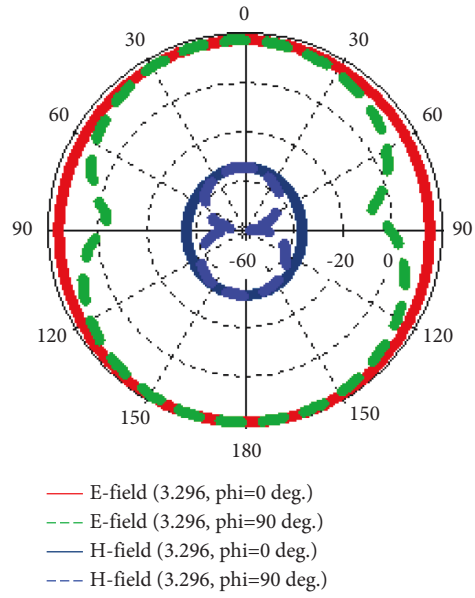

Figure 10: E-field and H-field of the prototype.

slight deviation of measured efficiency from the simulated efficiency which may happen due to the soldering error and port defect. From the graph, the maximum efficiency of the prototype is high (simulated is 95% and measured is 92%) which reveals that the designed MPA emits most of the input signal. The value of simulated efficiency ranges from 93% to 97% and measured efficiency ranges from 78% to 92% over the whole bandwidth. The impedance (real and imaginary part) is demonstrated in Figure 14. The real part and the imaginary part values are 53.35 Ω and −0.28 Ω, respectively, at 3.29 GHz. That means the impedance matching is upright for the fabricated prototype with respect to the reference 50 Ω SMA connector. A comparison Table 2 is incorporated to buttress the strength of the proposed design. Most of the cited designs have higher volume and lower efficiency than our proposed antenna. From Table 2, it can be conferred that

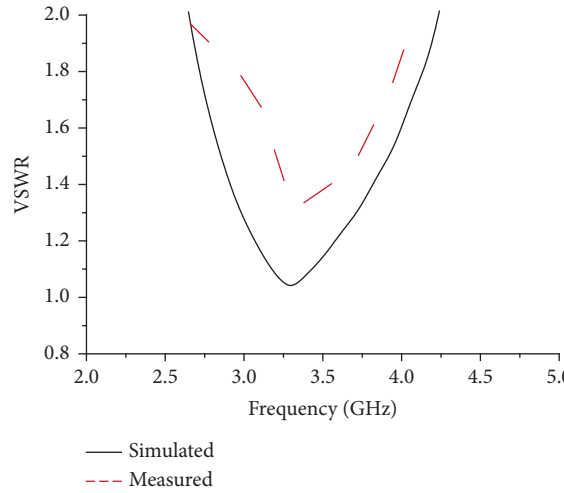

Figure 11: VSWR.

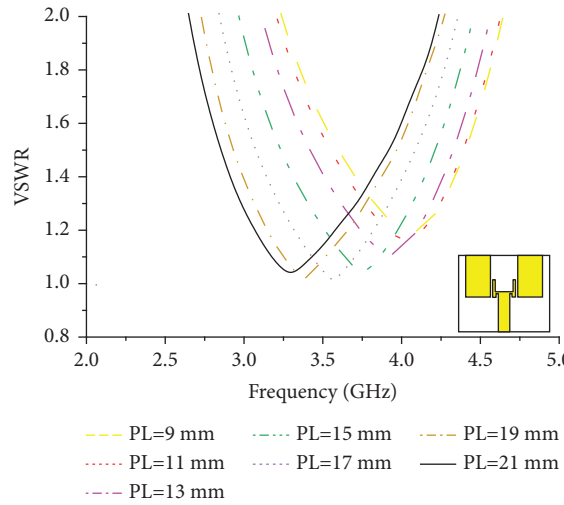

Figure 12: Variation of the VSWR for different length of parasitic element on the ground plane (P_L).

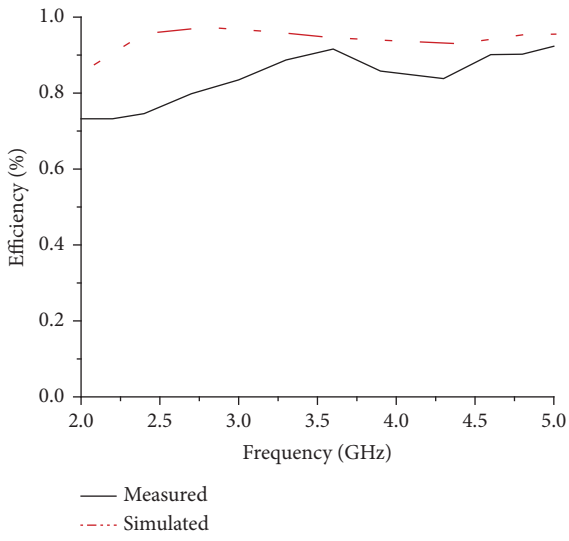

Figure 13: Radiation efficiency of the MPA.

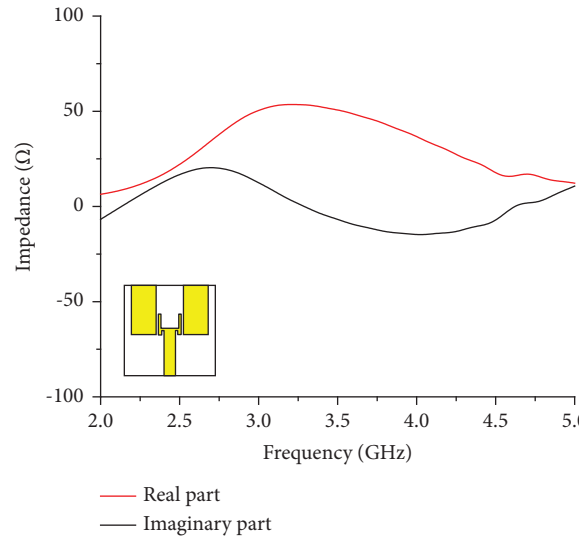

Figure 14: Z parameters of the MPA.

Table 2: Comparison table.

Index	Reference No.													This work
	[22]	[23]	[24]	[25]	[26]	[27]	[28]	[29]	[30]	[31]	[32]	[33]	[34]	
Physical size ($L \times W \times h$) mm^3	$40 \times 60 \times 1.52$	$46 \times 46 \times 3.175$	$35 \times 35 \times *$	$78 \times 58 \times 0.9$	$40 \times 30 \times 1.6$	$130 \times 130 \times *$	$22.5 \times 10.7 \times 1.6$	$45 \times 45 \times 1.0$	$48 \times 35 \times 1.62$	$36 \times 36 \times 4$	$34 \times 34 \times 3.2$	$150 \times 80 \times 0.8$	$90 \times 90 \times *$	$40 \times 40 \times 1.575$
Electrical size	$0.27\lambda \times 0.4\lambda$	$0.37\lambda \times 0.37\lambda$	$0.39\lambda \times 0.39\lambda$	$0.99\lambda \times 0.73\lambda$	$0.44\lambda \times 0.33\lambda$	$1.19\lambda \times 1.19\lambda$	$0.26\lambda \times 0.12\lambda$	$0.27\lambda \times 0.27\lambda$	$0.3\lambda \times 0.22\lambda$	$0.34\lambda \times 0.34\lambda$	$0.35\lambda \times 0.35\lambda$	$0.64\lambda \times 0.34\lambda$	$0.97\lambda \times 0.97\lambda$	$0.36\lambda \times 0.36\lambda$
Substrate material	Rogers RO4350 B ($\varepsilon_r = 3.48$)	Rogers RT ($\varepsilon_r = 2.2$)	ECCOSTOCK HIK ($\varepsilon_r = 10$)	PET ($\varepsilon_r = 3.2$)	FR-4	FR-4	FR-4 ($\varepsilon_r = 4.3$)	FR-4 ($\varepsilon_r = 4.4$)	FR-4 ($\varepsilon_r = 4.3$)	FR-4 ($\varepsilon_r = 4.4$)	FR-4 ($\varepsilon_r = 4.3$)	FR-4 ($\varepsilon_r = 4.5$)	Rogers RO4003C ($\varepsilon_r = 3.38$), Taconic TLX-9 ($\varepsilon_r = 2.5$)	Rogers RT 5880 ($\varepsilon_r = 2.2$)
Operating frequency range (GHz)	2–5	2.44–2.54, 3.19–3.55	3.30–4.38	3.89–5.9	3.28–4.0	2.75–5.45	3.4–4.2	1.82–2.92, 3.15–4.75	1.85–3.8	2.8–3.81	~3.1–3.75	~1.27–1.5, ~2.2–2.5, ~3.5–4.2	3.24–3.8	2.67–4.20
Maximum gain (dB)	7.14	~4	6	3	2.5	8.4	2.3	7.5	4.044	4.08	3.8	5	10.43	3.92
BW (GHz)	3	0.1, 0.36	1.08	2.01	0.72	2.7	0.8	0.1, 1.6	1.95	1.01	0.65	0.23, 0.3, 0.7	0.56	1.53
Radiation efficiency (%)	80	—	—	~80	—	~80	73	—	92	—	—	80	—	95
Applied methods	Metamaterial, slot	ENGTL metamaterials	DRA, parasitic	CPW fed	Partial ground	Balun	Log-periodic patch	Non-centred L-shaped	Metamaterial	Aperture coupled	Slot, PIN diode	Stub, open slot	Metasurface	Parasitic, partial ground

*Not mentioned.

the proposed design has a very well balanced set of radiation characteristics with a lower volume for Sub-6 GHz applications.

4. Conclusion

The fabricated omni-directional MPA has the ability to cover the Sub-6 GHz (N77 and N78) band for 5G applications and WiMAX rel 2 applications. The volume of the antenna is $40 \times 40 \times 1.575 = 2520\,\text{mm}^3$ which is made by Rogers RT 5880 and simulated by the CST-MWS suite. The simulated bandwidth and measured bandwidth of the MPA are 1.53 GHz (2.67 GHz–4.20 GHz) and 1.48 GHz (2.67 GHz–4.15 GHz) with a suitable return loss profile. The antenna has a good far field radiation pattern with good gain and directivity. Over the exhaustive bandwidth, the VSWR satisfies $1 < \text{VSWR} < 2$. The simulated and measured VSWR are 1.04 and 1.32 at the resonance point. The inset feeding technique, partial ground plane, and parasitic elements make the antenna more suitable for Sub-6 GHz application. It can also be used for WiMAX rel 2. The average radiation efficiencies of the proposed MPA are approximately 95% (simulated) and 92% (measured) over the working band. Due to the good agreement between simulated and measured results as well as wide range of frequency coverage, the designed omni-directional inset fed MPA may be taken into account as an excellent model for Sub-6 GHz applications.

Data Availability

The data used to support the findings of this study are included within the article.

Conflicts of Interest

The authors declare that they have no conflicts of interest.

References

[1] Q. Amjad, A. Kamran, F. Tariq, and R. Karim, "Design and characterization of a slot based patch antenna for sub-6 GHz 5G applications," in *Proceedings of the 2nd Int'l Conf. on Latest trends in Electrical Engineering and Computing Technologies*, pp. 1–6, Singapore, July 2019.

[2] A. A. Althuwayb, "MTM- and SIW-inspired bowtie antenna loaded with AMC for 5G mm-wave applications," *International Journal of Antennas and Propagation*, vol. 2021, Article ID 6658819, 7 pages, 2021.

[3] L. C. Paul, H. K. Saha, T. K. Roy, R. Azim, and M. T. Islam, "A wideband inset-fed simple patch antenna for sub-6 GHz band Applications," in *Proceedings of the 2022 International Conference on Innovations in Science, Engineering and Technology (ICISET)*, pp. 106–110, Dubai (UAE), November 2022.

[4] I. Ishteyaq, I. Shah Masoodi, and K. Muzaffar, "A compact double-band planar printed slot antenna for sub-6 GHz 5G wireless applications," *International Journal of Microwave and Wireless Technologies*, vol. 13, no. 5, pp. 469–477, 2020.

[5] R. A. Sadeghzadeh, M. Alibakhshi-Kenari, and M. Naser-Moghadasi, "UWB antenna based on SCRLH-TLs for portable wireless devices," *Microwave and Optical Technology Letters*, vol. 58, no. 1, pp. 69–71, 2015.

[6] L. C. Paul, M. H. Ali, R. Azim, and T. K. Roy, "A triple T-topped planar antenna for 5G/WiMAX applications," *2021 3rd International Conference on Sustainable Technologies for Industry 4.0 (STI)*, vol. 4, no. 0, pp. 1–5, 2021.

[7] L. C. Paul, H. K. Saha, T. Rani, R. Azim, M. T. Islam, and M. Samsuzzaman, "A dual band semi-circular patch antenna for WiMAX and WiFi-5/6 applications," *International Journal of Communication Systems*, vol. 2022, Article ID e5357, 2022.

[8] L. C. Paul, M. T. R. Jim, T. Rani, M. S. Rahman, M. Samsuzzaman, and R. Azim, "A H-shaped slotted circular patch antenna for sub-6 GHz applications," in *Proceedings of the 2022 International Conference on Innovations in Science, Engineering and Technology*, pp. 217–221, Chittagong, Bangladesh, February 2022.

[9] B. Huang, M. Li, W. Lin, J. Zhang, G. Zhang, and F. Wu, "A compact slotted patch hybrid-mode antenna for sub-6 GHz communication," *International Journal of Antennas and Propagation*, vol. 2020, Article ID 8262361, 8 pages, 2020.

[10] M. K. Islam, A. Madanayake, and S. Bhardwaj, "Design of maximum-gain dielectric lens antenna via phase center analysis," *International Applied Computational Electromagnetics Society Symposium*, pp. 1–4, 2021.

[11] R. Azim, R. Akter, A. K. M. M. H. Siddique, L. C. Paul, and M. T. Islam, "Circular patch planar ultra-wideband antenna for 5G sub-6 GHz wireless communication applications," *Journal of Optoelectronics and Advanced Materials*, vol. 23, no. 3-4, pp. 127–133, 2021.

[12] R. Azim, A. M. H. Meaze, A. Affandi et al., "A multi-slotted antenna for LTE/5G Sub-6 GHz wireless communication applications," *International Journal of Microwave and Wireless Technologies*, vol. 13, no. 5, pp. 486–496, 2020.

[13] U. Farooq, "A compact monopole patch antenna for future sub 6 GHz 5G wireless applications," in *Proceedings of the IEEE International Symposium on Antennas and Propagation and North American Radio Science Meeting*, pp. 1715-1716, Montreal, Canada, July 2020.

[14] L. C. Paul, S. C. Das, M. N. Hossain, and W. S. Lee, "A wideband rose-shaped patch antenna with a ground slot for sub-6 GHz applications," *2021 IEEE Indian Conference on Antennas and Propagation (InCAP)*, pp. 901–904, 2021.

[15] X. Tang, "Ultra-wideband patch antenna for sub-6 GHz 5G communications," in *Proceedings of the Int'l Workshop on Electromagnetics: Applications and Student Innovation Competition*, pp. 1–3, Qingdao, China, August 2019.

[16] W. A. Awan, N. Hussain, A. Ghaffar, A. Zaidi, and X. J. Li, "A compact flexible antennas for ISM and 5G sub-6- GHz band Application," in *Proceedings of the WSA 2020; 24th International ITG Workshop on Smart Antennas*, pp. 1–3, Hamburg, Germany, February 2020.

[17] S. Ullah, I. Ahmad, Y. Raheem, S. Ullah, T. Ahmad, and U. Habib, "Hexagonal shaped CPW feed based frequency reconfigurable antenna for WLAN and sub-6 GHz 5G applications," in *Proceedings of the 2020 International Conference on Emerging Trends in Smart Technologies (ICETST)*, pp. 1–4, Karachi, Pakistan, March 2020.

[18] A. A. Althuwayb, "Enhanced radiation gain and efficiency of a metamaterial inspired wideband microstrip antenna using substrate integrated waveguide technology for sub-6 GHz wireless communication systems," *Microwave and Optical Technology Letters*, vol. 63, no. 7, pp. 1892–1898, 2021.

[19] M. A. Kenari, "Printed planar patch antennas based on metamaterial," *International Journal of Electronics Letters*, vol. 2, no. 1, pp. 37–42, 2014.

[20] S. Murugan, "Compact square patch antenna for 5G communication," in *Proceedings of the 2nd Int'l Conf. on Data, Engineering and Applications*, pp. 1–3, Bhopal, India, February 2020.

[21] S. S. A. Ankan, L. C. Paul, T. Rani, S. C. Das, and W. S. Lee, "A planar monopole antenna array with partial ground plane and slots for sub-6 GHz wireless applications," *2022 IEEE Wireless Antenna and Microwave Symposium (WAMS)*, vol. 2022, pp. 1–5, 2022.

[22] A. Hoque, M. T. Islam, and A. F. Almutairi, "Low-profile slotted metamaterial antenna based on Bi slot microstrip patch for 5G application," *Sensors*, vol. 20, no. 11, p. 3323, 2020.

[23] S. Nelaturi, "ENGTL based antenna for Wi-Fi and 5G," *Analog Integrated Circuits and Signal Processing*, vol. 107, no. 1, pp. 165–170, 2021.

[24] J. Iqbal, U. Illahi, M. N. M. Yasin, M. A. Albreem, and M. F. Akbar, "Bandwidth enhancement by using parasitic patch on dielectric resonator antenna for sub-6 GHz 5G NR bands application," *Alexandria Engineering Journal*, vol. 61, no. 6, pp. 5021–5032, 2022.

[25] A. Desai, T. Upadhyaya, J. Patel, R. Patel, and M. Palandoken, "Flexible CPW fed transparent antenna for WLAN and sub-6 GHz 5G applications," *Microwave and Optical Technology Letters*, vol. 62, no. 5, pp. 2090–2103, 2020.

[26] A. Kapoor, R. Mishra, and P. Kumar, "Compact wideband-printed antenna for sub-6 GHz fifth-generation applications," *International Journal on Smart Sensing and Intelligent Systems*, vol. 13, no. 1, pp. 1–10, 2020.

[27] B. Huang, W. Lin, J. Huang, J. Zhang, G. Zhang, and F. Wu, "A patch/dipole hybrid-mode antenna for sub-6GHz communication," *Sensors*, vol. 19, no. 6, pp. 1358–1367, 2019.

[28] M. Yerlikaya, S. S. Gültekin, and D. Uzer, "A novel design of a compact wideband patch antenna for sub-6 GHz fifth-generation mobile systems," *International Advanced Researches and Engineering Journal*, vol. 4, no. 2, pp. 129–133, 2020.

[29] Z. Yu, L. Huang, Q. Gao, and B. He, "A compact dual-band wideband circularly polarized microstrip antenna for sub-6G application," *Progress In Electromagnetics Research Letters*, vol. 100, pp. 99–107, 2021.

[30] H. Singh, N. Mittal, A. Gupta, Y. Kumar, M. Woźniak, and A. Waheed, "Metamaterial integrated folded dipole antenna with low SAR for 4G, 5G and NB-IoT applications," *Electronics*, vol. 10, no. 21, pp. 2612–2620, 2021.

[31] R. Swetha and A. Lokam, "Novel design and characterization of wide band hook shaped aperture coupled circularly polarized antenna for 5G application," *Progress In Electromagnetics Research C*, vol. 113, pp. 161–175, 2021.

[32] Y. I. Al-Yasir, A. S. Abdullah, N. Ojaroudi Parchin, R. A. Abd-Alhameed, and J. M. Noras, "A new polarization-reconfigurable antenna for 5G applications," *Electronics*, vol. 7, no. 11, pp. 293–299, 2018.

[33] M. Khalifa, L. Khashan, H. Badawy, and F. Ibrahim, "Broadband printed-dipole antenna for 4G/5G smartphones," *Journal of Physics: Conference Series*, vol. 1447, no. 1, pp. 012049–9, 2020.

[34] J. Park, M. Jeong, N. Hussain, S. Rhee, S. Park, and N. Kim, "A low-profile high-gain filtering antenna for fifth generation systems based on nonuniform metasurface," *Microwave and Optical Technology Letters*, vol. 61, no. 11, pp. 2513–2519, 2019.